Journal of ELECTRONIC MATERIALS, Vol. 42, No. 7, 2013
DOI: 10.1007/s11664-013-2535-x

Stacked Micro Heat Exchange System for Optimized Thermal Coupling of MicroTEGs

N. WOJTAS,[1,3] M. GRAB,[1] W. GLATZ,[2] and C. HIEROLD[1]

1.—Micro and Nanosystems, ETH Zurich, Tannenstrasse 3, 8092 Zurich, Switzerland. 2.—greenTEG GmbH, Technoparkstrasse 1, 8005 Zurich, Switzerland. 3.—e-mail: nwojtas@ethz.ch

This study presents modeling and experimental results of micro thermoelectric generators (μTEGs) integrated into a multilayer micro heat exchange system. The multilayer configuration benefits from low heat transfer resistances at small fluid flow rates and at the same time from low required pumping powers. The compact stacked power device allows for high net output power per volume, and therefore a reduction in size, weight, and cost compared with conventional large-scale heat exchangers. The influence of the boundary conditions and the system design parameters on the net output power of the micro heat exchange system was investigated by simulation. The theoretical results showed a major impact of the microchannel dimensions and the μTEG thickness on the overall output performance of the system. By adapting the applied fluid flow rate, the system's net power output can be maximized for varying operating temperatures. Experimental measurements of the cross-flow micro heat exchange system were in good agreement with the performed simulations. A net μTEG output power of 62.9 mW/cm^2 was measured for a double-layer system at an applied water inlet temperature difference of 60 K with a Bi_2Te_3 μTEG (ZT of 0.12), resulting in a net volumetric efficiency factor of 37.2 W/m^3/K^2.

Key words: Micro thermoelectric generator, micro heat exchange system, thermal coupling, waste heat recovery, volumetric efficiency factor

INTRODUCTION

Large amounts of energy in the form of hot fluids are wasted during electric power generation and industrial processing. Due to significant progress in the development of high-ZT thermoelectric materials,[1,2] low-temperature thermoelectric waste heat recovery from industrial plants is considered to be a promising approach to enhance overall system efficiency.[3] To maximize the recovered net power, the entire thermoelectric heat exchange system must be optimized. This includes minimization of thermal contact resistances for high effective temperature gradients across the thermoelectric generator and adapting the heat exchanger and generator design parameters (e.g., thermal resistance matching[4]).

(Received July 7, 2012; accepted February 7, 2013; published online May 4, 2013)

Several numerical models of fluidic heat exchange systems in combination with TEG modules have been presented for different system designs and complexities.[5–8] However, the advantages of a microfluidic thermal interface, overall system optimization including most of the relevant system parameters (e.g., TEG thermal resistances), and net power output estimations have not been considered. A few experimental investigations of stacked TEGs between parallel-plate heat exchangers have been reported for industrial applications,[9–11] where considerable output powers of 500 W (at ΔT = 207 K)[11] or high volumetric efficiencies of 3 W/m^3/K^2 (at ΔT = 120 K, ZT = 0.225)[9] were reached. The proposed systems, however, were large, heavy, and not optimized with respect to net power or thermal and geometric system parameters.

By reducing the dimensions of the heat transfer interface to the micrometer scale, the efficiency of

the heat exchange system, and therefore the thermal coupling to the generator, can be significantly enhanced. Micro heat transfer systems (μHTSs) can achieve high heat flux densities with a compact system design.

This paper reports the design, simulation, and experimental results of a multilayer thermoelectric micro heat exchange system. The working principle is illustrated in the schematic drawing in Fig. 1a. Bi_2Te_3 μTEGs are alternately stacked between cold and hot micro heat transfer systems. Each μHTS consists of three functional layers: two copper microchannel layers for efficient heat dissipation or supply, and a polymer manifold layer for uniform fluid distribution. This configuration combines the advantages of very low heat transfer resistances enabled by the microchannels, and small pressure losses due to the short fluid paths inside the channels.[12]

Minimization of heat transfer resistances simultaneously allows for reduction of the necessary TEG thickness for optimal thermal matching. This results in overall cost, size, and weight reduction as well as large potential for high-heat-flux heat exchange applications.

MODELING AND SIMULATIONS

For the design and optimization of the thermoelectric heat exchange system, a one-dimensional numerical model was implemented and the influence of the μHTS and the μTEG parameters on the net output power performance was investigated.

The generic part of the μHTS model is based on Ref. 12. The presented thermoelectric heat exchange model consists of periodic unit cells of one μTEG and two μHTSs. The equivalent thermal resistance model is depicted in Fig. 1b. The μTEG thermal resistance is composed of the resistance of the thermocouples R_{TC}, the isolating matrix around the thermocouples R_{iso}, and the interconnect resistance R_{intercon} at both sides. The total heat transfer resistance R_{HTS} consists of the conductive resistance through the microchannels R_{cond}, the convective resistance at the fluid–channel interface R_{conv}, and the fluid resistance due to its limited heat capacity R_{hc}:

$$R_{\mathrm{HTS}} = R_{\mathrm{cond}} + R_{\mathrm{conv}} + R_{\mathrm{hc}}. \tag{1}$$

The conductive thermal resistance is defined as

$$R_{\mathrm{cond}} = \frac{t_{\mathrm{base}}}{\lambda_{\mathrm{Cu}}}, \tag{2}$$

where t_{base} is the thickness of the microchannel chip base and λ_{Cu} is the thermal conductivity of copper. The convective resistance is given by

$$R_{\mathrm{conv}} = \frac{1}{\bar{h}_{\mathrm{ch}} A_{\mathrm{ch}}}, \tag{3}$$

where $\bar{h}_{\mathrm{ch}}$ is the average convective heat transfer coefficient and A_{ch} is the surface area of the microchannels. The fluid resistance can be expressed as

$$R_{\mathrm{HC}} = \frac{1}{\dot{m} c_{\mathrm{p}}} = \frac{1}{\dot{V} \rho c_{\mathrm{p}}}, \tag{4}$$

where $\dot{m}$ is the mass flow rate, $\dot{V}$ is the volumetric flow rate, ρ is the fluid density, and c_{p} is the specific heat capacity.

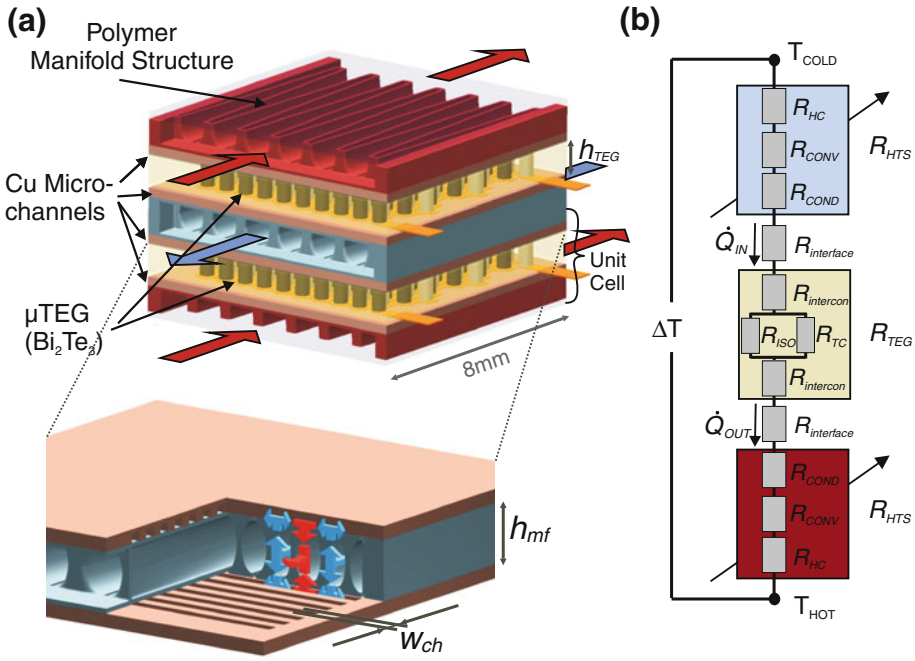

Fig. 1. (a) Schematic drawing of a thermoelectric heat exchange system with enlarged view of the multilayer heat transfer system. (b) Equivalent thermal resistance network of one unit cell.

Between the μTEG and the two μHTSs an interface resistance $R_{\text{interface}}$ is added to account for the electric isolation of the μTEG and the thermal paste for improved thermal contact.

The μTEG output power was calculated under matched electric load conditions according to Ref. 13, where Joule heating and Peltier losses were included

$$P_{\text{out}} = \frac{U_0^2}{4R_{\text{el}}} = \frac{(m\alpha)^2}{4R_{\text{el}}}\Delta T_{\text{g}}^2, \tag{5}$$

where U_0 is the output voltage under load, R_{el} is the electrical resistance of the generator, m is the number of thermocouples inside the TEG, α is the Seebeck coefficient, and ΔT_{g} is the temperature gradient across the generator.

The necessary pumping power through the system was computed from the hydrodynamic resistance of the μHTS as

$$P_{\text{pump}} = \dot{V}\Delta p_{\text{HTS}} = \dot{V}(\Delta p_{\text{ch}} + \Delta p_{\text{mf}}), \tag{6}$$

where Δp_{HTS} is the total pressure loss of the μHTS, consisting of the hydrodynamic losses inside the microchannels Δp_{ch} and the manifold distribution channels Δp_{mf}.

The pumping power was subtracted from the μTEG output power in order to determine the net power. The influence of the temperature-dependent fluid parameters on the thermal resistance and pressure loss calculations in the μHTS was accounted for by introducing a discrete temperature profile inside the microchannels. Due to the small heat exchange between the manifold and the microchannel, a gradual fluid temperature change along the manifold channels occurs. Therefore, the temperature profile is represented by a flow-dependent weight function of the average inlet temperature. Infrared measurements were used to determine the temperature profile.

The thermoelectric conversion efficiency of the μTEG is defined as

$$\eta_{\text{TE}} = \frac{\dot{Q}_{\text{in}} - \dot{Q}_{\text{out}}}{\dot{Q}_{\text{in}}} = \frac{P_{\text{out}}}{\dot{Q}_{\text{in}}}, \tag{7}$$

where $\dot{Q}_{\text{in}}$ and $\dot{Q}_{\text{out}}$ are the heat fluxes entering and exiting the μTEG, respectively. The second law efficiency is expressed as

$$\eta_{2\text{nd}} = \frac{\eta_{\text{TE}}}{\eta_{\text{Carnot}}}. \tag{8}$$

To compare different thermoelectric heat exchange systems with different dimensions and applied fluid inlet temperatures, a volumetric efficiency factor was introduced as

$$\text{VEF} = \frac{P_{\text{out}}}{V\Delta T^2}, \tag{9}$$

where V is the system volume. Equally, the net volumetric efficiency factor can be computed by inserting the net output power $P_{\text{out,net}}$ of the system into Eq. 9.

The implemented model allows for analysis and optimization of all geometric parameters and most material properties. The system parameters with the greatest impact on the net output power are discussed herein.

All relevant system dimensions and material parameters used for the simulations and measurements of the single- (unit cell) and double-layer micro heat exchange systems are summarized in Table I. The standard simulation parameters of the single-layer heat exchange system (bold values) were set to match the parameters of the μHTS and μTEG devices characterized later in this study. The module ZT is defined as the figure of merit of the μTEG, where the entire generator's resistance (including electric contact resistance and the interconnect resistance) is used for the electric resistivity calculation.

Figure 2 shows the influence of the applied flow rate and different μHTS design parameter values on the system's unit cell performance. In Fig. 2a the total heat transfer resistance R_{HTS} and corresponding pumping power P_{pump} (cold and hot side) are plotted against different cold and hot fluid flow rates. While R_{HTS} decreases with rising flow rates (mainly due to a reduction in R_{hc} caused by the enhanced volumetric mass flow), the corresponding pumping power increases (due to a rise in the hydrodynamic resistance). The trade-off between those two parameters results in an optimal flow rate where the net output power is maximized. Figure 2b shows the dependence of the net output power on the hot and cold flow rates for a fluid inlet

Table I. Bi_2Te_3 μTEG and μHTS parameters used for simulations and measurements

	μTEG Parameters					μHTS Parameters		
	Module ZT (–)	**R_{el} (Ω)**	**R_{TEG} (cm^2K/W)**	**α (μV/K)**	**h_{TEG} (μm)**	**w_{ch} (μm)**	**h_{ch} μm)**	**h_{mf} cold/hot (mm)**
Single-layer	**0.12** ± 0.01	**1.2** ± 0.01	**2.9** ± 0.3	**212** ± 5	**215** ± 5	**45** ± 2	**190** ± 10	**1/1** ± 0.05
Variations*	0.03–0.84	–	–	100–550	10–400	20–80	100–300	–
Double-layer	0.14 ± 0.01	1.2 ± 0.01	2.9 ± 0.3	230 ± 7	215 ± 5	45 ± 2	190 ± 10	0.5/1 ± 0.05

*Parameter variations used for the simulations of the single-layer heat exchange system

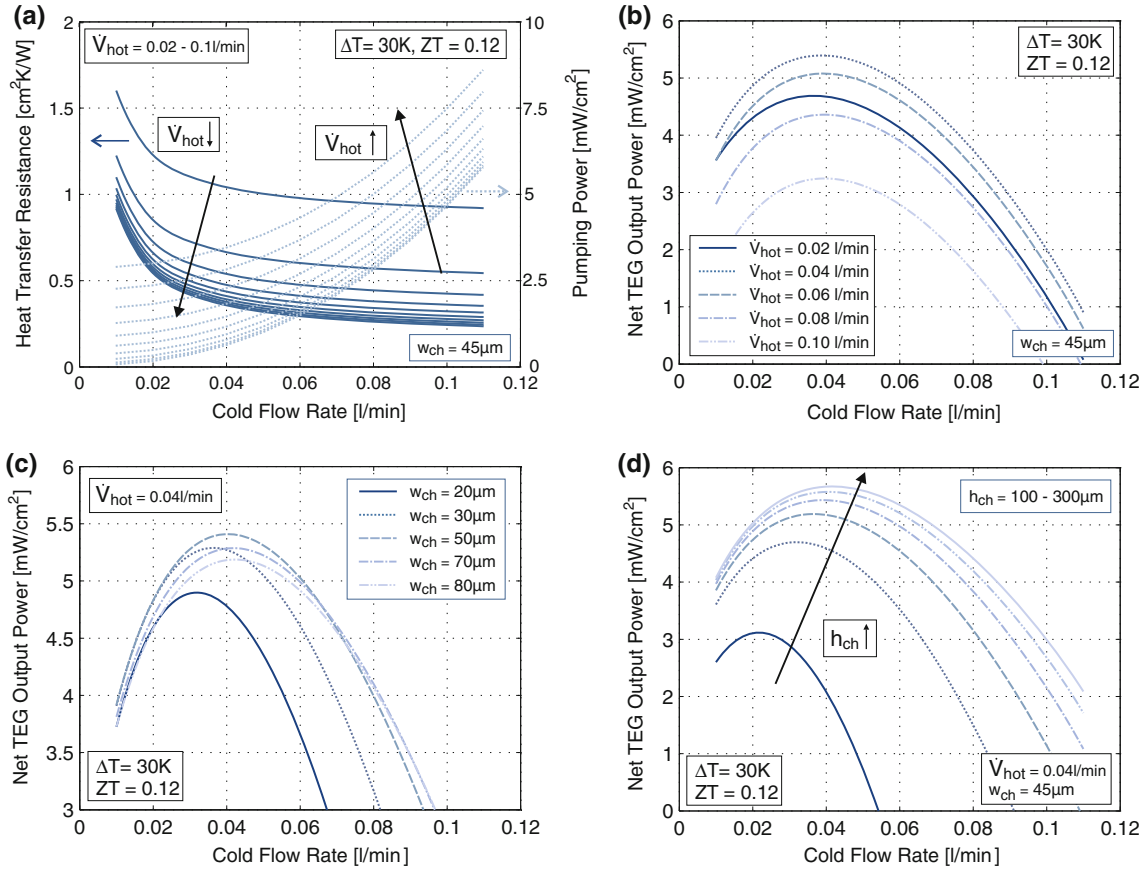

Fig. 2. Unit cell simulations of the thermoelectric heat exchange system with a Bi_2Te_3 μTEG for different cold flow rates at a fluid inlet temperature difference of ΔT = 30 K. (a) Heat transfer resistance and corresponding pumping power as a function of the hot flow rate. Net output power as a function of (b) the hot flow rate, (c) the microchannel width, and (d) the microchannel height.

temperature difference of 30 K. While the heat transfer is insufficient at small flow rates and the large pumping power outweighs the enhanced heat transfer at larger flow rates, a moderate cold and hot flow rate of 0.04 l/min is optimal. In Fig. 2c the influence of the microchannel width on the net power is depicted. With increasing channel width, the heat transfer resistance increases due to reduced convection and the pumping power decreases due to the induced higher shear forces. This results in an optimal microchannel width depending on the fluid flow rate and fluid inlet temperature difference applied. In Fig. 2d the microchannel height is plotted against the cold fluid flow rate. With increasing channel height, the net output power increases and the optimal flow rate shifts to higher values. The former can be explained by the increase of the convective surface area and by the reduced pumping power due to the increase of the hydrodynamic diameter. The latter is a result of the reduced influence of the pumping power relative to the μTEG output power.

When a greater fluid inlet temperature difference is applied, higher flow rates and smaller channel widths will result in optimal performance, since the effect of the heat transfer resistance on the power output increases and the relative impact of the pumping power on the net power decreases.

For the optimization of the overall system's net output performance, the μTEG dimensions and parameters also must be considered. In Fig. 3a, the effect of the μTEG thickness on the net output power (dark blue) and thermoelectric conversion efficiency of the μTEG η_{TE} (light blue) for three different fluid flow rates and inlet temperature differences ΔT is shown. With increasing ΔT applied, the maximal net output power point (marked in the figure) shifts towards higher fluid flow rates and thinner μTEGs. The optimal μTEG thickness results from the matching of the μTEG thermal resistance R_{TEG} with the sum of all the contact resistances R_{con}[4] (although a small shift due to Joule and Peltier losses exists)

$$R_{TEG} \cong R_{con} = R_{HTS_{cold}} + R_{HTS_{hot}} + 2R_{interface}. \quad (10)$$

Due to an increase of the optimal flow rate with increasing applied ΔT and corresponding reduction of the cold and hot heat transfer resistances, the optimal μTEG thickness decreases as well.

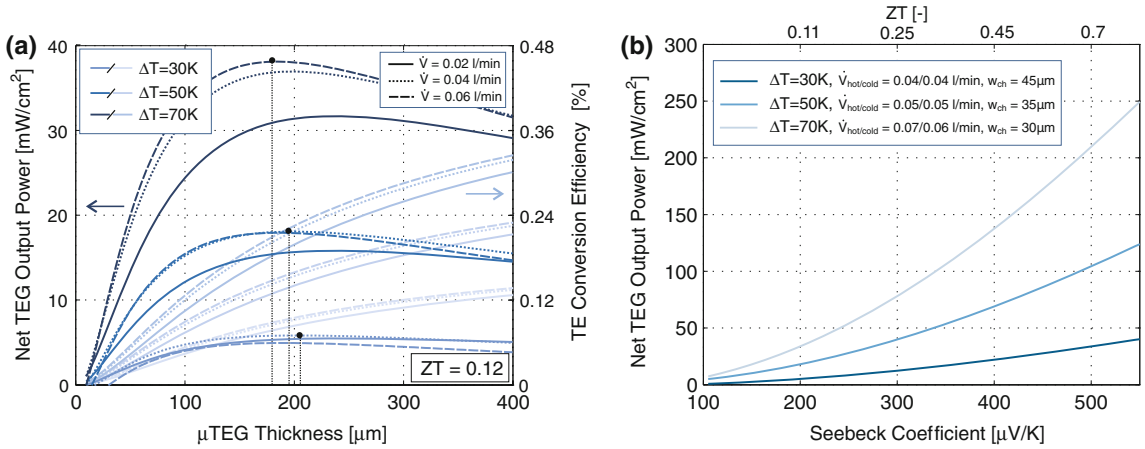

Fig. 3. Unit cell simulations of the thermoelectric heat exchange system with a Bi_2Te_3 μTEG for three different fluid inlet temperature differences ΔT with optimal microchannel widths. (a) Net μTEG output power (dark blue) and thermoelectric conversion efficiency (light blue) as a function of μTEG thickness and different fluid flow rates. (b) Net μTEG output power as a function of the Seebeck voltage (ZT 0.03 to 0.85) at optimal fluid flow rates.

The thermoelectric conversion efficiency of the μTEG η_{TE} increases with rising fluid flow rates and thicker μTEGs. The former can be explained by the increase in output power with enhanced thermal coupling, whereas the latter is a result of a continuous reduction of the heat flux $\dot{Q}_{in}$ entering the generator.

To demonstrate the potential of an improved thermoelectric material, the μTEG net power output is plotted in Fig. 3b as a function of the Seebeck coefficient (of one thermocouple) for three different inlet temperature differences. The fluid flow rates and microchannel widths are set to the optimal value at the corresponding ΔT, where the net power is maximized.

EXPERIMENTAL MEASUREMENTS

First experimental measurements were performed on single- (unit cell) and double-layer micro heat exchange systems. The μHTS prototypes were fabricated by means of high-aspect-ratio photolithography and electrochemical deposition for the microchannels[14] and microstereolithography for the manifold channels. The fabrication of the μTEGs is described in Ref. 15. The samples were clamped with constant pressure and characterized in a controlled fluid flow loop. The μTEG output power was calculated from the measured Seebeck voltage and the μTEG resistance (see Eq. 5), and the pumping power was calculated from the measured pressure losses and volumetric flow rate (see Eq. 6).

Figure 4 shows the measured (markers) and computed (lines) μTEG output performance for a single- (Fig. 4a–c) and double-layer (Fig. 4d) thermoelectric heat exchange system. The μTEG and system parameters used for the experimental measurements and corresponding simulations can be found in Table I.

In Fig. 4a, the μTEG output power is depicted as a function of different cold and hot fluid flow rates for an applied ΔT of 30 K. With increasing flow, the total output power increases due to a reduction of the heat transfer resistance R_{HTS} (see Fig. 2a). When the pumping power is subtracted, an optimal flow rate can be found (according to Fig. 2b).

In Fig. 4c, the net output power is plotted as a function of the fluid flow rates for fluid inlet temperatures between 10 K and 60 K. At the lowest applied ΔT of 10 K, the pumping power outweighs the μTEG output and no positive net power can be reached. With increasing ΔT, the power gain and the optimal flow point increase. Figure 4d shows the net output power of a two-layer system as a function of the applied ΔT for different fluid flow rates. The power output was approximately doubled compared with the single-layer system. The slight differences in the net performance result from the nonidentical system parameters (Table I). The reduced manifold channel height in the double-sided heat transfer system (limited by the fabrication process) caused an increase in pumping power, showing its biggest impact at low temperatures and high flow rates. On the other hand, the improved net power at higher temperatures is due to the higher Seebeck coefficient of the μTEGs used.

The measurement results are in good agreement with the computed values. The largest deviations between simulations and measurements occur at higher temperatures. Those differences might be attributed to a Bi_2Te_3 Seebeck coefficient increase with temperature (not accounted for in the model), potential changes in $R_{interface}$, and a possible increased error of the fluid flow measurements caused by operation outside the specified temperature range (for ΔT = 60 K only).

CONCLUSIONS

The potential of thermoelectric multilayer micro heat exchange systems for efficient power generation

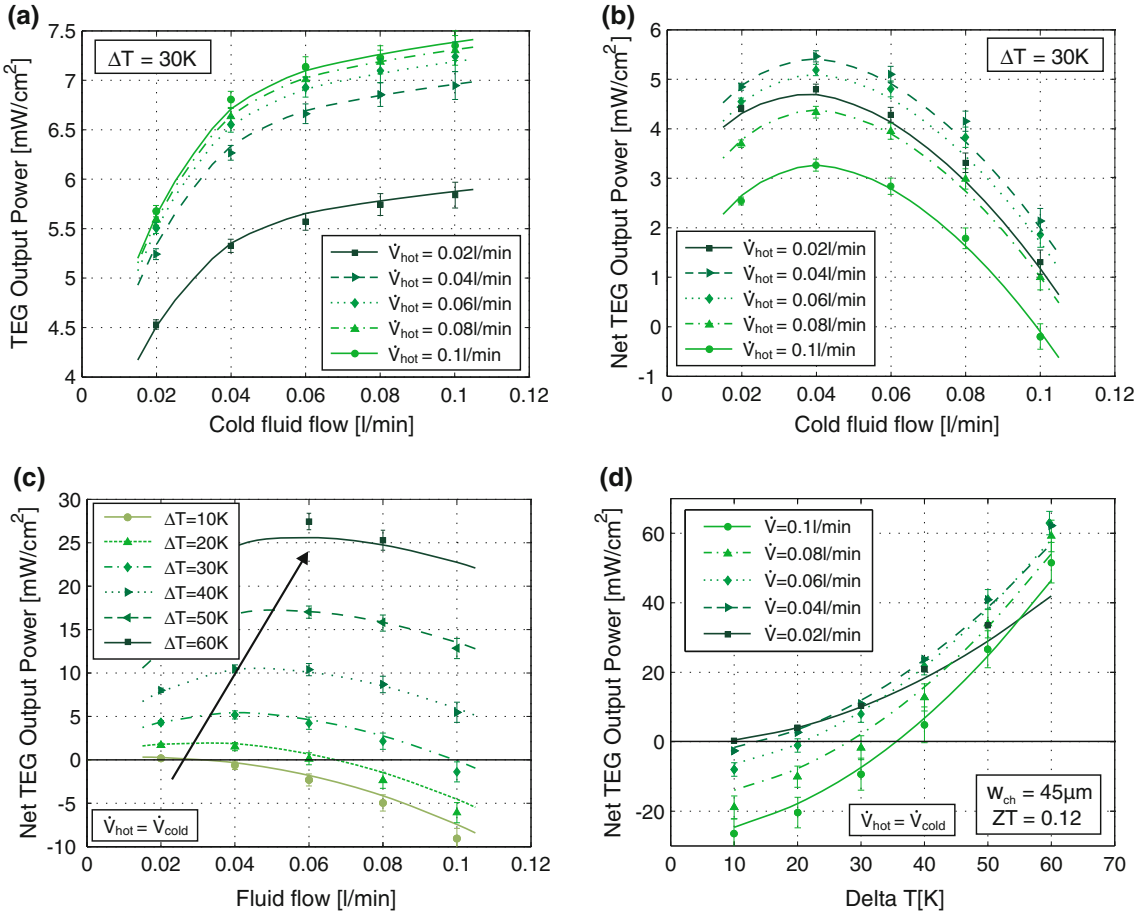

Fig. 4. Measurements (markers) and simulations (lines) of the thermoelectric heat exchange system with a Bi_2Te_3 μTEG. (a) Total and (b) net output power of a single-layer system for different flow rates at a fluid inlet temperature difference ΔT = 30 K. Net output power of a (c) single- and (d) double-layer system for different ΔT values and different fluid flow rates.

was demonstrated in this study. A one-dimensional numerical model for system design and optimization was implemented, and the influence of several system parameters on the net power output of the thermoelectric heat exchange systems was investigated. For the overall system optimization, the coupled influence of design parameters and boundary conditions on the net system performance has to be considered.

It was shown that, for specific fluid inlet temperature differences ΔT, optimal operating conditions, micro heat exchange system parameters, and μTEG parameters can be determined.

First experimental results were in good agreement with the simulated system behavior. Net output power of 62.9 mW/cm^2 (132.5 mW/cm^3) was measured with a Bi_2Te_3 μTEG module (ZT of 0.12) at a ΔT of 60 K, resulting in a net second law efficiency of 1.8% and net volumetric efficiency factor of 37.2 W/m^3/K^2, which is an order of magnitude higher than reported elsewhere.

By improving the thermoelectric material properties and upscaling the system, thermoelectric low-temperature waste heat recovery in industrial applications becomes feasible.

ACKNOWLEDGEMENTS

The authors would like to thank Thomas Helbling for helpful discussions, ETH Zurich for financial support, and Proform AG for manifold fabrication.

REFERENCES

1. R. Venkatasubramanian, E. Siivola, T. Colpitts, and B. O'Quinn, *Nature* 413, 6856 (2001).
2. K.F. Hsu, S. Loo, F. Guo, W. Chen, J.S. Dyck, C. Uher, T. Hogan, E.K. Polychroniadis, and M.G. Kanatzidis, *Science* 303, 5659 (2004).
3. D.M. Rowe, *Int. J. Innov. Energy Syst. Power* 1, 1 (2006).
4. J.W. Stevens, *Energy Convers. Manage.* 42, 6 (2001).
5. J.L. Yu and H. Zhao, *J. Power Sour.* 172, 1 (2007).
6. F.K. Meng, L.G. Chen, and F.R. Sun, *Energy* 36, 5 (2011).
7. S. Belanger and L. Gosselin, *Energy Convers. Manage.* 52, 8–9 (2011).
8. J. Esarte, G. Min, and D.M. Rowe, *J. Power Sour.* 93, 1–2 (2001).
9. X. Niu, J.L. Yu, and S.Z. Wang, *J. Power Sour.* 188, 2 (2009).
10. A. Tsuyoshi and K. Matsuura, *Electr. Eng. Jpn.* 141, 1 (2002).
11. D.T. Crane, J.W. LaGrandeur, F. Harris, and L.E. Bell, *J. Electron. Mater.* 38, 7 (2009).

12. W. Escher, D. Poulikakos, T. Brunschwiler, and B. Michel, *J. Heat Trans. ASME* 132, 8 (2010).
13. M. Strasser, R. Aigner, C. Lauterbach, T.F. Sturm, M. Franosch, and G. Wachutka, *Sens. Actuators A* 114, 2–3 (2004).
14. N. Wojtas, E. Schwyter, W. Glatz, S. Kühne, W. Escher, and C. Hierold, *Sens. Actuators A: Phys.* 188, (2012).
15. W. Glatz, E. Schwyter, L. Durrer, and C. Hierold, *JMEMS* 18, 3 (2009).